PHYSICAL REVIEW A **69**, 031801(R) (2004)

(2+1)-dimensional stable spatial Raman solitons

M. Y. Shverdin, D. D. Yavuz, and D. R. Walker
Edward L. Ginzton Laboratory, Stanford University, Stanford, California 94305, USA
(Received 8 September 2003; published 3 March 2004)

We analyze the formation, propagation, and interaction of stable two-frequency (2+1)-dimensional solitons, formed in a Raman media driven near maximum molecular coherence. The propagating light is trapped in the two transverse dimensions.

DOI: 10.1103/PhysRevA.69.031801 PACS number(s): 42.65.Dr, 42.65.Tg, 42.50.Gy, 42.65.Jx

The generation of stable spatial optical solitons is of great interest due to the variety of the solitons' interactions, their particlelike characteristics, and their potential technological applications [1]. Spatial soliton formation requires a balance between the beam's tendencies to self-focus and diffract. In bulk [three-dimensional (3D)] media, such propagation is unstable, unless the focusing nonlinearity saturates with the intensity [2,3]. Experimentally, spatial (2+1)-dimensional solitons have been demonstrated in a variety of physical systems, including photorefractive media [4,5], quadratic media [6,7], and saturable Kerr media [8,9]. While the equations governing the various types of self-trapped waves differ, the fundamental propagation and interaction properties remain the same [10].

We have recently proposed a method for generating spatial Raman solitons [11]. We adiabatically prepare a Raman transition in a single eigenstate near maximum molecular coherence by driving the medium with two opposite circularly polarized laser fields whose frequency difference is slightly detuned from the Raman resonance (Fig. 1). Depending on the sign of the detuning $\Delta\omega$, the adiabatically established molecular coherence is either in phase or out of phase with the strong two-photon drive. Angular-momentum conservation rules prevent Stokes and anti-Stokes sideband generation [12]. Instead the molecular coherence modifies the refractive indices of the driving lasers [13–15] and leads to either focusing or defocusing, depending on the sign on the detuning [16]. An appropriate choice of the input intensities and the two-photon detuning from the Raman resonance leads to bright ($\Delta\omega>0$) or dark ($\Delta\omega<0$) soliton formation.

In this paper, we extend the analysis of bright Raman solitons to three spatial dimensions. We numerically and theoretically demonstrate that these solitary waves are stable to perturbations and survive soliton-soliton collisions. Stability is achieved by operating near maximum molecular coherence, $|\rho_{ab}|\approx 1/2$, and thereby saturating the Raman nonlinearity with the laser intensity. Adiabatic preparation of near maximum coherence is essential and ties this work to broadband Raman generation [17] and electromagnetically induced transparency [18].

Following Ref. [19], we consider a model Raman system excited with opposite circularly polarized pump, E_p, and Stokes, E_s, lasers, oscillating at frequencies ω_p and ω_s. The analysis applies to beams propagating along the z axis with the electric field oscillating in two transverse dimensions (x and y). We assume no time variation in the propagating beam profiles. Experimentally, this can be realized using flat-top pulses. The slowly varying envelope propagation equations for the pump and the Stokes beams at steady state are

$$2k_p\frac{\partial E_p}{\partial z}+j\left(\frac{\partial^2 E_p}{\partial x^2}+\frac{\partial^2 E_p}{\partial y^2}\right)=-j2\eta\hbar\omega_p k_p N(a_p\rho_{aa}E_p + d_p\rho_{bb}E_p+b^*\rho_{ab}E_s),$$

$$2k_s\frac{\partial E_s}{\partial z}+j\left(\frac{\partial^2 E_s}{\partial x^2}+\frac{\partial^2 E_s}{\partial y^2}\right)=-j2\eta\hbar\omega_s k_s N(a_s\rho_{aa}E_s+d_s\rho_{bb}E_s + b\rho_{ab}^* E_p), \quad (1)$$

where N is the molecule number density and $\eta=(\mu/\epsilon_0)^{1/2}$. The population in the two states $|a\rangle$ and $|b\rangle$ are given by ρ_{aa} and ρ_{bb}. The molecular coherence of the two levels, ρ_{ab} (off-diagonal density-matrix element), is responsible for the intensity dependence of the refractive index. The dispersion coefficients at the pump and the Stokes frequencies, a_p, a_s, d_p, d_s, and the coupling coefficient b, are calculated elsewhere [19]. When the matrix elements of the Hamiltonian that describes the evolution of the molecular system vary slowly compared to the separation of the eigenvalues of the

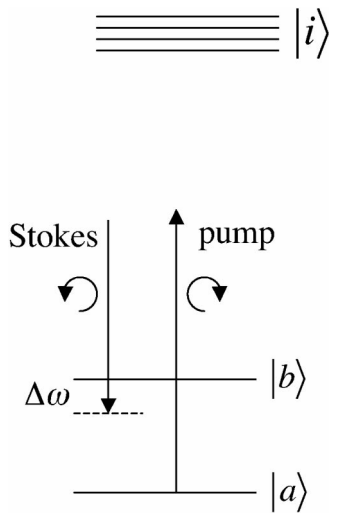

FIG. 1. Energy-level diagram of a sample Raman system driven by two opposite circular polarized fields. As shown, the two-photon detuning is positive leading to self-focusing.

Hamiltonian, the molecular medium can be prepared adiabatically in an eigenstate that is smoothly connected to the ground state. Examining only the bright soliton case ($\Delta\omega > 0$), the density-matrix elements of this eigenstate are

$$\rho_{ab} = \frac{B/2}{\sqrt{|B|^2 + (\Delta\omega - D/2 + A/2)^2}},$$

$$\rho_{aa} = \cos^2\left(\frac{\theta}{2}\right); \quad \rho_{bb} = \sin^2\left(\frac{\theta}{2}\right) \tag{2}$$

with $A = a_p|E_p|^2 + a_s|E_s|^2$, $B = bE_pE_s^*$, $D = d_p|E_p|^2 + d_s|E_s|^2$, and $\tan\theta = 2|B|/(2\Delta\omega - D + A)$, resulting in the refractive index enhancement. The effect of collisional dephasing may be accounted for by adding an imaginary term $j\Gamma$ to the two-photon detuning $\Delta\omega$. The dephasing rate of the Raman transition determines the loss of the driving fields and, therefore, sets the maximum pulse width.

In the analytical portion below, but not in the numerical portion of this work we make the following assumptions: (1) The solitons are cylindrically symmetric; (2) since the driving lasers are far detuned from one-photon resonances, we take all dispersion constants to be equal, $a_p = a_s = d_p = d_s \equiv a_0$; (3) since the Raman frequency is much smaller than the driving lasers' frequencies, we take $\omega_p = \omega_s \equiv \omega_0$ and $k_p = k_s \equiv k_0$. Letting $E_p(z=0) = E_s(z=0) = E_0(z=0)$, and using the expression for ρ_{ab} from Eq. (2) we transform Eq. (1):

$$2k_0\frac{\partial E_0}{\partial z} + j\left(\frac{1}{r}\frac{\partial E_0}{\partial r} + \frac{\partial^2 E_0}{\partial r^2}\right) = -j\kappa\frac{|E_0|^2}{\sqrt{1 + |b|^2|E_0|^4/\Delta\omega^2}}E_0, \tag{3}$$

where $\kappa = \eta\hbar\omega_0 k_0 N|b|^2/\Delta\omega$. In 3D, only a numerical solution exists to this equation [8].

The self-trapped solution to Eq. (3) must have the form $E_0(r,z) = F(r)\exp(-j\xi z)$. We determine the relationship between the wave vector ξ and radial beam profile $F(r)$, by substituting the expression for $E_0(r,z)$ into Eq. (3),

$$\frac{\partial^2 F}{\partial r^2} + \frac{1}{r}\frac{\partial F}{\partial r} + \kappa\frac{F^3}{\sqrt{1 + |b|^2F^4/\Delta\omega^2}} - 2\xi k_0 F = 0. \tag{4}$$

We determine the magnitude of ξ by choosing peak soliton amplitude $F(r=0) = F_0$. Then the boundary conditions are $F(r\to\infty) = 0$, $(\partial F/\partial r)(r\to\infty) = 0$, and $(\partial F/\partial r)(r=0) = 0$. We vary the values of ξ and numerically integrate Eq. (4) until the computed spatial profile $F(r)$ satisfies the given boundary conditions. In Fig. 2, we calculate several soliton profiles corresponding to various peak molecular coherence values. The soliton's beam size varies inversely with the field amplitude. As the peak intensity decreases, the saturation is reduced, and the soliton shape approaches the calculation by Chiao *et al.* [8]. We find that both the value of ξ and the total power increase as the peak soliton intensity is raised.

The stability of the solitons of Fig. 2 against small perturbations can be shown by using the well-known Vakhitov-Kolokolov stability criterion [20,21]. In Fig. 3, we numerically calculate the power contained in each soliton, $P(\xi) = 2\pi\int F(\xi)^2 r\, dr$, and plot versus the parameter ξ. This calculation shows that $\partial P/\partial\xi > 0$ which, according to the Vakhitov-Kolokolov criterion, proves the stability of the soliton. The stability is a consequence of the saturation term on the right-hand side of Eq. (3).

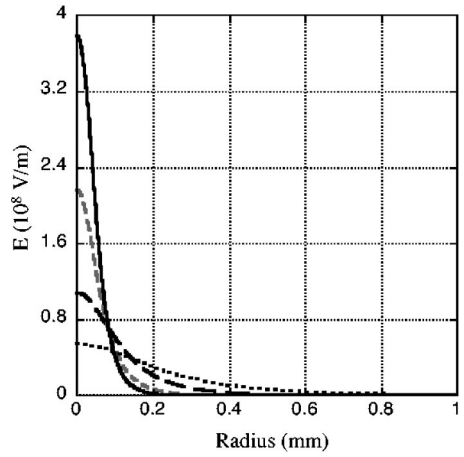

FIG. 2. Initial soliton profiles calculated by numerical integration of Eq. (4). The shapes are cylindrically symmetric and correspond to peak coherence values of 0.02 (dotted line), 0.09 (long dashed), 0.29 (short dashed), 0.45 (solid). The corresponding values of $\xi = (1.2, 4.8, 19.0, 49.5)$ m^{-1}, respectively.

We proceed with soliton propagation and collision dynamics in a real molecular system. Here, we neither assume cylindrical symmetry nor make the dispersive approximations of Eq. (3). We consider the $|\nu''=0, J''=0\rangle \to |\nu'=0, J'=2\rangle$ rotational transition in molecular H_2 with $\omega_b - \omega_a = 354$ cm^{-1}. The simulation parameters are similar to those in our recent experiment [16]: molecular density $N = 2.68\times10^{19}$ molecules/cm^3 and the two-photon detuning is $\Delta\omega = 1$ GHz. The wavelengths of the pump and the Stokes beams are 800 nm and 823 nm, respectively. In our simulation, we use the method of lines. Starting with the initial values, we evaluate the transverse derivatives and the pump and the Stokes field amplitudes of Eq. (1) on a 2D grid. We then advance the field envelopes in z, using a four-step Runge-Kutta method.

Dispersion modifies the soliton profiles of Fig. 2. The propagating waveform converges to a solitary wave when the initial beam parameters differ from the exact soliton shape.

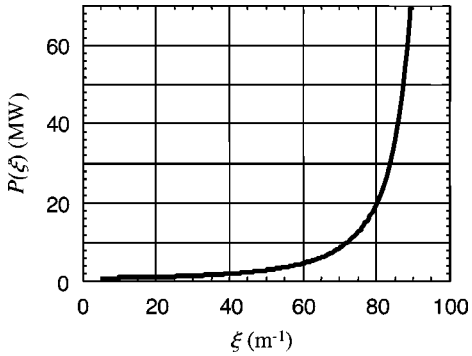

FIG. 3. Vakhitov-Kolokolov stability criterion. The total power in the soliton beam is shown as a function of the parameter ξ in Eq. (4).

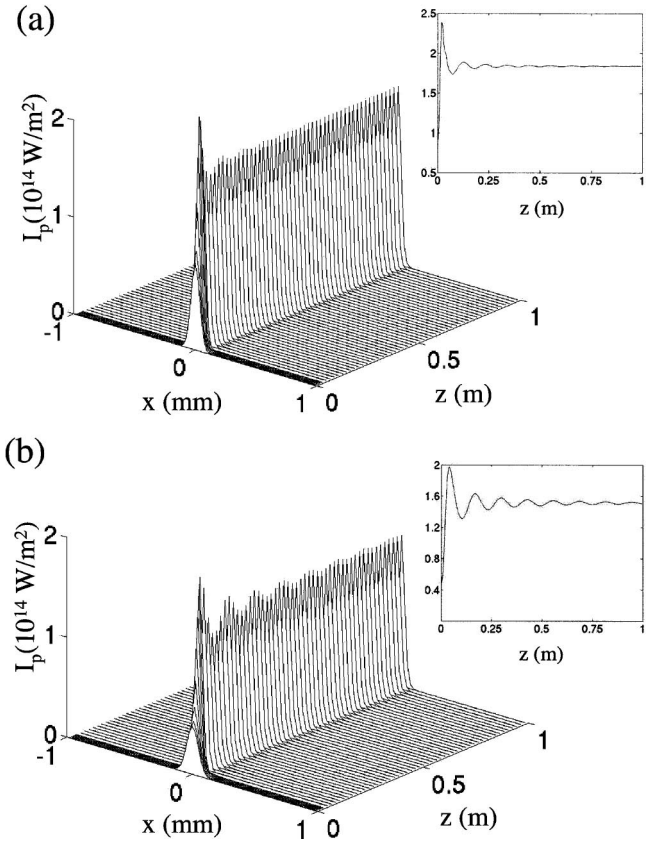

FIG. 4. Initial Gaussian profiles propagating through a 1 m long H_2 cell. In the absence of Raman self-focusing, the spatial width of the beam would increase by a factor of 50 in part (a), and a factor of 30 in part (b). The inset figure shows the peak beam intensity versus propagation distance. The beam breathes as it converges to a soliton. The initial peak coherence is 0.43 in part (a), and 0.29 in part (b). The convergence distance in (a) is shorter than in part (b).

We examine soliton stability and convergence by propagating initial Gaussian pulses of similar intensity and beam width to the shapes in Fig. 2. In Fig. 4, we plot the field intensity of two pump pulses versus propagation distance along the z axis. The inset figure represents the corresponding peak field intensity versus distance. In part (a), the pulse corresponds to an initial intensity of 6.2×10^9 GW/cm^2 and full width half maximum (FWHM) of 0.10 mm. In part (b), the pulse corresponds to an initial intensity of 3.3×10^9 GW/cm^2 and FWHM of 0.13 mm. As the Gaussian pulses propagate, their shapes breathe as the beams converge to respective soliton shapes. The breathing behavior is clearly apparent in the inset plots. The beams are centered at the origin in the x-y plane and the three-dimensional plots are generated by taking $y=0$ for each value of z. The peak soliton intensity is a factor of 1.4 higher than the initial profile's intensity in Fig. 4(a), and a factor of 1.8 higher in Fig. 4(b). Since the total power is conserved, the beam narrows in profile as the peak intensity increases. The amplitude of the breathing depends on the mismatch of the initial intensity profile from the corresponding soliton shape. In Fig. 4(b), breathing becomes negligible in $\approx$50 cm, but in part (b), the breathing continues for $\approx$1 m. This convergence distance is determined by the peak coherence value. At higher coherence, the response of the system increases and the equilibrium is reached in a shorter distance. These figures clearly demonstrate the stability of Raman solitons to the perturbations of the beam shapes.

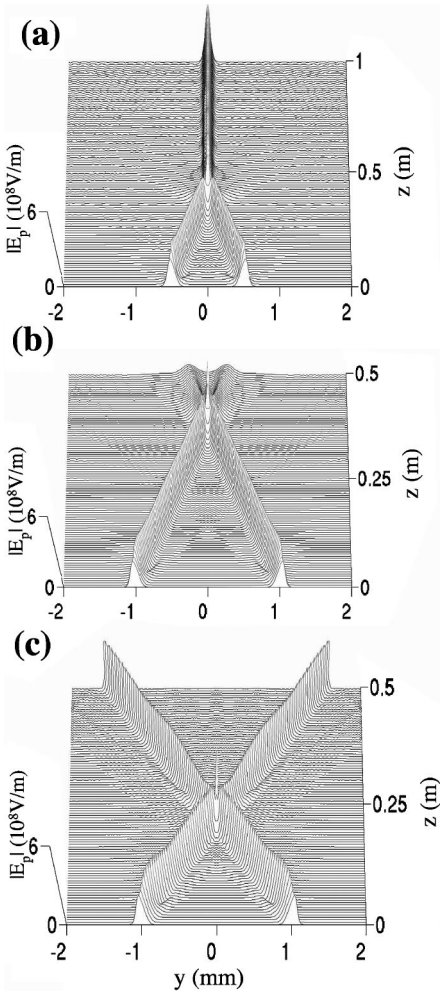

FIG. 5. Calculation of soliton collisions for three cases. (a) Inelastic collision: beams collide and fuse into one soliton. The beams are launched at the collision angle of 0.003 rad. (b) Beams collide and disappear; collision angle of 0.006 rad. (c) Elastic collision: beams collide, pass through each other, and remain solitons; collision angle of 0.012 rad.

We now proceed with numerical studies of soliton-soliton collisions. In an elastic collision, two solitons pass through each other, maintaining their shape. In an inelastic collision, two solitons fuse after colliding and become a single soliton. The outcome of a soliton interaction is determined by the angle of the collision θ [10,22]. When the collision angle exceeds some critical angle θ_c the collision is elastic. When $\theta<\theta_c$, the solitons fuse together. When $\theta\approx\theta_c$ solitons disappear after colliding, as the diffraction overcomes self-focusing.

In Fig. 5, all three possible interaction outcomes are shown. At an initial peak coherence of 0.39 (7.3 GW/cm^2), two Gaussian pulses converge to soliton profiles before colliding. For the given parameters, $\theta_c\approx0.006$ rad [23]. The beams approach each other as solitons at angles θ

$=0.003$ rad, 0.006 rad, and 0.012 rad, respectively. In part (a), the solitons collide and fuse into one; in part (b), the solitons collide and disappear; in part (c), the solitons collide and pass through each other. In the elastic collision case, after interaction, the emerging waveform begins to breathe as it converges to a soliton profile. In our simulations, we pick the initial phase profiles so that the two input pulses propagate in the *y*-*z* plane. Choosing the origin to be in the middle of the cell, we center the input pulses at $(x,y,z)=(0,y_0,0)$ and $(0,-y_0,0)$ and propagate the pulses toward each other along the *y* axis. The displayed figures show the electric-field amplitude versus *y* and *z* at a fixed value of *x*. For each value of *z*, the plot is then a slice along *y* at a value of *x* where the electric field peaks.

In summary, we have presented the numerical and theoretical analysis of two-frequency Raman solitons in a molecular system. We have shown that these solitons are stable in the two transverse propagation dimensions. In our analysis we ignored the time dependence of the pump and the Stokes pulses and we also assumed no dephasing of the Raman transition. There are several potential practical limitations to the Raman solitons that require further study. First, to prepare the molecular coherence the medium absorbs photons from the pump field and emits into the Stokes field at the leading edge of the pulses. At the trailing edge, photons are absorbed at the Stokes field and emitted into the pump field. The resulting delay of the time envelope of the pump pulse with respect to the Stokes pulse sets the minimum-energy requirement to form a soliton [24]. The number of photons in the leading edge of the pump pulse must equal the number of molecules contained in the volume swept by the pulse, $V_{swept}=\frac{1}{2}L\pi w_0^2$, where w_0 is the soliton spot size and L is the distance the pulse propagates through the medium. Second, the dephasing of the Raman transition will lead to some loss of the pump and the Stokes fields. Hence, the pulse width must be shorter than the dephasing time ($\approx$100 nsec for the parameters in this paper, at 77 K, and can be increased by further cooling). Finally, the leading edges of the pump and the Stokes pulses will diffract. While the exact behavior requires a time domain analysis, we can estimate the spot size of the leading edges at a distance $L \gg z_R$ after the beginning of the cell, as $w(L)=w_0L/z_R$, where $z_R=\pi w_0^2/\lambda$ (assuming the worst case scenario of a freely diffracting beam). As the leading edge diffracts, the energy is deposited into a larger volume of molecules than required for soliton propagation. This raises the minimum-energy requirement by a factor of $(L/z_R)^2$.

ACKNOWLEDGMENTS

The authors thank Steve Harris and Vlatko Balic for many helpful discussions. The authors would also like to thank Sergei Polyakov for an early suggestion of the soliton stability. This work was supported by the U.S. Office of Naval Research, the U.S. Army Research Office, and the U.S. Air Force Office of Scientific Research. D.R.W. also acknowledges support from the Fannie and John Hertz Foundation.

[1] G. I. Stegeman and M. Segev, Phys. Today **51**(8), 42 (1998).
[2] Y. Silberberg, Opt. Lett. **15**, 1282 (1990).
[3] A. W. Snyder, D. J. Mitchell, L. Poladian, and F. Ladouceur, Opt. Lett. **16**, 21 (1991).
[4] M. Segev, B. Crosignani, A. Yariv, and B. Fischer, Phys. Rev. Lett. **68**, 923 (1992).
[5] G. Duree *et al.*, Phys. Rev. Lett. **71**, 533 (1993).
[6] Y. N. Karamzin and A. P. Sukhorukov, Zh. Eksp. Teor. Fiz. Pis'ma Red. **20**, 734 (1974) [Sov. Phys. JETP **41**, 414 (1976)].
[7] W. E. Torruellas *et al.*, Phys. Rev. Lett. **74**, 5036 (1995).
[8] R. Y. Chiao, E. Garmire, and C. H. Townes, Phys. Rev. Lett. **13**, 479 (1964).
[9] A. Barthelemy, S. Maneuf, and C. Froehly, Opt. Commun. **55**, 201 (1985).
[10] G. I. Stegeman and M. Segev, Science **286**, 1518 (1999).
[11] D. D. Yavuz, D. R. Walker, and M. Y. Shverdin, Phys. Rev. A **67**, 041803 (2003).
[12] A. V. Sokolov, S. J. Sharpe, M. Shverdin, D. R. Walker, D. D. Yavuz, G. Y. Yin, and S. E. Harris, Opt. Lett. **26**, 725 (2001).
[13] S. E. Harris, Opt. Lett. **19**, 2018 (1994).
[14] V. S. Butylkin, A. E. Kaplan, and Y. G. Khronopulo, Opt. Spectrosc. **31**, 120 (1972).
[15] D. Grischkowsky, M. M. T. Loy, and P. F. Liao, Phys. Rev. A **12**, 2514 (1975).
[16] D. R. Walker, D. D. Yavuz, M. Y. Shverdin, G. Y. Yin, A. V. Sokolov, and S. E. Harris, Opt. Lett. **27**, 2094 (2002).
[17] A. V. Sokolov, D. R. Walker, D. D. Yavuz, G. Y. Yin, and S. E. Harris, Phys. Rev. Lett. **85**, 562 (2000).
[18] S. E. Harris, Phys. Today **50**(7), 36 (1997).
[19] S. E. Harris and A. V. Sokolov, Phys. Rev. Lett. **81**, 2894 (1998).
[20] N. G. Vakhitov and A. A. Kolokolov, Radiophys. Quantum Electron. **16**, 783 (1973).
[21] S. Trillo and W. Torruellas, *Spatial Solitons* (Springer-Verlag, Berlin, 2001).
[22] A. V. Buryak and V. V. Steblina, J. Opt. Soc. Am. B **16**, 245 (1999).
[23] A high intensity propagating field can be said to create an effective waveguide in the media. A soliton will either escape or couple into the waveguide based on the refractive index difference and the collision angle. An elastic collision occurs for all $\theta > \theta_c$. We can approximate θ_c by calculating the refractive index difference between the regions of peak field intensity n_{max} and minimum field intensity n_{min}. Then $\theta_c \approx \pi/2 - \sin^{-1}(n_{min}/n_{max})$, where $n_{min}=1+(N\hbar/\epsilon_0)(a_p\rho_{aa}+d_p\rho_{bb})$, and $n_{max}=1+(N\hbar/\epsilon_0)[a_p\rho_{aa}+d_p\rho_{bb}+b\rho_{ab}(E_s/E_p)]$.
[24] S. E. Harris and Z.-F. Luo, Phys. Rev. A **52**, R928 (1995).